Size dependence in flux-flow Hall effect using time-dependent Ginzburg-Landau equations

Vineet Punyamoorty,[1] Aditya Malusare,[2] Shamashis Sengupta,[3] Sumiran Pujari [ORCID],[4] and Kasturi Saha [ORCID][1,*]

[1]*Department of Electrical Engineering, Indian Institute of Technology Bombay, Mumbai 400076, India*
[2]*Department of Physics and Astronomy, Purdue University, West Lafayette, Indiana 47907, USA*
[3]*Université Paris-Saclay, CNRS/IN2P3, IJCLab, 91405 Orsay, France*
[4]*Department of Physics, Indian Institute of Technology Bombay, Mumbai 400076, India*

We study the Hall effect in square, planar type-II superconductors using numerical simulations of time dependent Ginzburg-Landau (TDGL) equations. The Hall field in some type-II superconductors displays sign-change behavior at some magnetic fields due to the induced field of vortex flow when its contribution is strong enough to reverse the field direction. In this paper, we use modified TDGL equations which couple an externally applied current, and also incorporate normal-state and flux-flow Hall effects. We obtain the profile of Hall angle as a function of applied magnetic field for six different sizes ($l \times l$) of the superconductor: $l/\xi \in \{3, 5, 15, 20, 100, 200\}$. We obtain vastly different profiles for different size regimes, proving that size is an important parameter that determines Hall behavior. We find that electric field dynamics provide an insight into several anomalous features including a sign change of the Hall angle, and leads us to the precise transient behavior of the order parameter responsible for them.

I. INTRODUCTION

One of the most interesting aspects of superconducting systems is the physics of vortices. Advances in experimental methods have made it possible to probe type-II superconductors at small length scales where the behavior of individual vortices becomes visible. Vortices have been imaged with electron spins in diamonds [1,2], scanning superconducting quantum-interference devices [3,4], and Hall-probe magnetometry [5,6]. The behavior of a superconducting system is expected to vary significantly if its dimensions are reduced to be comparable to the coherence length. In this paper, we theoretically investigate the effect of finite size on the properties of vortices with numerical simulations of solutions of the time-dependent Ginzburg-Landau (TDGL) equations. The flux-flow Hall effect in square planar type-II superconductors is studied for different sample sizes, given by l/ξ ratio of 3, 5, 15, 20, 100, and 200 (where l is the length of the square and ξ is the superconducting coherence length). Sizes $l/\xi \in \{100, 200\}$ serve as representatives of the bulk regime. It will be seen that the electric field and Hall angle profiles under a unidirectional current are widely different depending upon the dimension of the superconductor.

Hall effect in superconductors has been observed to display anomalous properties below the critical temperature, most

significant of which is the sign reversal of Hall voltage at certain magnetic fields [7–9]. This could not be explained by either the phenomenological models of vortex flow of the time, namely, the Bardeen-Stephen (BS) model [10] and the Nozières-Vinen model [11], or by microscopic theory [12]. It was later proposed that the induced electric field of magnetic vortex flow could contribute to the Hall field and cause anomalous behavior [9]. Dorsey [12] and Kopnin *et al.* [13] proved, using analytical approximations of a modified TDGL system, that indeed sign reversal of Hall effect is possible under some circumstances. These theories make use of microscopic quantities (related to the electronic structure) to define the regimes of sign reversal. Alternatively, one may numerically compute the Hall effect in a superconducting sample governed by the modified TDGL system of Dorsey [12] and Kopnin *et al.* [13], and find the magnetic field regimes of sign reversal. This could provide insights into Hall effect behavior of a superconductor as a function of macroscopic quantities alone (e.g., GL parameter κ, sample size, etc.).

In this paper, we follow the alternative numerical route mentioned above, which is direct and does not resort to any analytical approximations. We first use standard TDGL equations [14–16] to numerically compute the time-varying order parameter of a planar superconductor in the vortex state. We benchmark our simulations by comparing the numerically obtained fluxoid value of each vortex against Φ_0, the superconducting flux quantum, as a rigorous test (Sec. III A). With these benchmarks in hand, we simulate a modified TDGL system that includes an externally applied current to probe the Hall effect in these systems. Importantly, we go beyond existing literature by incorporating the normal-state Hall conductivity and flux-flow terms into the dynamical equations that we numerically simulate. In this, we have taken

inspiration from the analytical works of Dorsey [12] and Kopnin *et al.* [13] (Sec. III B). Next, in Sec. III C, we study the resultant changes in flux flow and resultant induced electric fields based on the numerical simulation of our modified TDGL system. We compute the Hall angle profile for various sizes of the superconductor and find vastly different profiles. We find that transient electric fields and related order parameter behavior give us good insight into explaining the anomalous Hall effect.

II. THEORETICAL MODEL

The TDGL equations are [14–16]

$$\gamma\left(\hbar\frac{\partial\psi}{\partial t} + ie_s\Phi\psi\right) + \frac{1}{2m_s}\left(i\hbar\nabla + \frac{e_s}{c}\mathbf{A}\right)^2\psi + \alpha\psi$$
$$+ \beta|\psi|^2\psi = 0, \tag{1a}$$

$$\nu\left(\frac{1}{c}\frac{\partial\mathbf{A}}{\partial t} + \nabla\Phi\right) + \frac{ie_s\hbar}{2m_s}(\psi^*\nabla\psi - \psi\nabla\psi^*) + \frac{e_s^2}{m_sc}|\psi|^2\mathbf{A}$$
$$+ \frac{c}{4\pi}\nabla\times\nabla\times\mathbf{A} = 0, \tag{1b}$$

where ψ is the complex-valued order parameter, α and β are the phenomenological parameters of Ginzburg-Landau theory [17,18], and ϕ, $\mathbf{A}$ are the electric and magnetic potentials, respectively. ν is the normal-state conductivity and γ is a relaxation constant for the order parameter. The charge and mass of Cooper pairs are denoted by $e_s = 2e$ and $m_s = 2m_e$, respectively. In the second equation above, which is basically the Maxwell's law $\nabla\times\mathbf{B} = \frac{1}{c}\frac{\partial\mathbf{E}}{\partial t} + \frac{4\pi}{c}\mathbf{J}$, we have used the standard approximation of $\partial_t\mathbf{E}\sim 0$ because of the low characteristic frequencies involved [16] in the vortex dynamics responsible for the Hall effects.

A. Gauge invariance and normalization

For an arbitrary function $\chi(x, y, t)$ with well-defined spatial and time derivatives, the gauge invariance can be expressed as $(\psi\to\psi e^{i\kappa\chi}, \mathbf{A}\to\mathbf{A}+\nabla\chi, \phi\to\phi-\frac{\partial\chi}{\partial t})$. We choose the zero electric potential gauge (i.e., $\phi = 0$) [14,15,19]. The physical quantities in Eqs. (1) are renormalized as follows:

$$\frac{x}{\xi}\to x, \quad \frac{t}{\gamma\hbar/(-\alpha)}\to t, \quad \frac{\mathbf{A}}{\sqrt{2}H_c\xi}\to\mathbf{A}, \quad \frac{\psi}{\sqrt{-\alpha/\beta}}\to\psi, \tag{2}$$

where $H_c = \sqrt{\frac{4\pi\alpha^2}{\beta}}$ and ξ is the GL coherence length [19]. In the chosen gauge, the resulting dimensionless equations applicable over the superconducting domain are

$$\frac{\partial\psi}{\partial t} + \left(i\nabla + \frac{1}{\kappa}\mathbf{A}\right)^2\psi - (1 - |\psi|^2)\psi = 0, \tag{3a}$$

$$\sigma\frac{\partial\mathbf{A}}{\partial t} + \nabla\times\nabla\times\mathbf{A} + \frac{i}{2\kappa}(\psi^*\nabla\psi - \psi\nabla\psi^*)$$
$$+ \frac{1}{\kappa^2}|\psi|^2\mathbf{A} = 0, \tag{3b}$$

where κ is the GL parameter and σ is normalized normal-state conductivity. When the sample is surrounded by vacuum
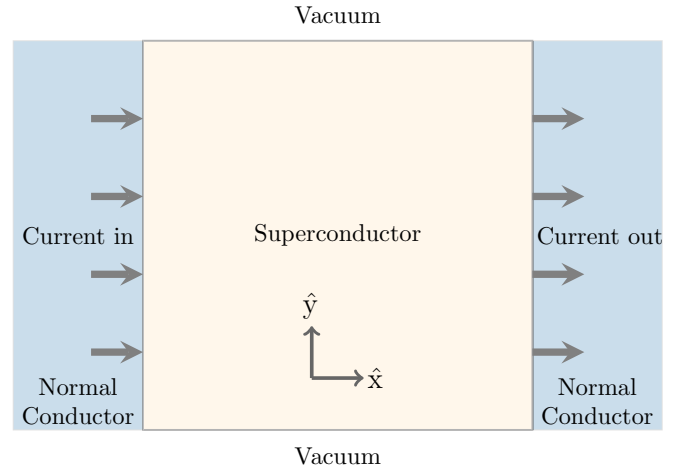

FIG. 1. Schematic representation of our simulation domain when an external current is applied – $l\times l$ square superconductor with metallic contacts on the left and right, and vacuum at top and bottom. Current $\mathbf{J}_a$ is applied along $\hat{\mathbf{x}}$ and magnetic field $\mathbf{H}_{\text{ext}}$ along $\hat{\mathbf{z}}$.

on all sides and no external current is passed, the following boundary conditions (BCs) apply [14,19–21]:

$$\nabla\times\mathbf{A} = \mathbf{H}_{\text{ext}}, \quad \left(i\nabla + \frac{1}{\kappa}\mathbf{A}\right)\psi\cdot\mathbf{n} = 0, \quad -\sigma\frac{\partial\mathbf{A}}{\partial t}\cdot\mathbf{n} = 0 \tag{4}$$

(where $\mathbf{H}_{\text{ext}}$ is the externally applied magnetic field, perpendicular to the sample). The first condition imposes continuity of transverse magnetic field across the boundary, while the second and third ensure that neither supercurrent nor normal current crosses the boundary, respectively.

In the case of a thin film superconductor (in xy plane), the electric field in the domain of the sample is of the form $E_x\hat{\mathbf{x}} + E_y\hat{\mathbf{y}}$ due to charge neutrality, and magnetic field is of the form $H\hat{\mathbf{z}}$. In principle, one also needs to solve Maxwell's equation $\nabla\times\nabla\times\mathbf{A} = 0$ (considering vacuum) in the surrounding domain [19]. However, in the case of two-dimensional samples with perpendicularly applied magnetic field, as in our system, solving the interior problem Eqs. (3) alone is sufficient to a good approximation [15,22]. For reference, the full problem and its BCs are discussed in Refs. [14] and [19,23].

B. Inclusion of externally applied current

Including an externally applied transport current in the TDGL system entails two tasks: (a) accounting for the magnetic field induced by the transport current and (b) modifying the BCs Eq. (4) to account for flow of normal current across boundaries. The former can be achieved by modifying the first BC to $\nabla\times\mathbf{A} = \mathbf{H}_{\text{tot}}$ where $\mathbf{H}_{\text{tot}} = \mathbf{H}_{\text{ext}} + \mathbf{H}_c$ is the sum of applied ($\mathbf{H}_{\text{ext}}$) and induced ($\mathbf{H}_c$) magnetic fields [20]. $\mathbf{H}_c$ is to be computed from the current profile (a function of ψ, $\mathbf{A}$), making the system self-consistent. However, an approximation is frequently used in literature [20,24–27] to simplify the computation of $\mathbf{H}_c$: the current profile is assumed to be a uniform band, which reduces $\mathbf{H}_c$ to a simple expression involving $\mathbf{J}_a$, the applied (uniform) current density. In this paper, $\mathbf{J}_a$ is assumed to be in the $+\hat{\mathbf{x}}$ direction (Fig. 1), which gives us $\mathbf{H}_c$

along all four boundaries as $\mathbf{H}_c^{\text{top, bottom}} = \pm W J_a / 2\, \hat{\mathbf{z}}$ (where W is the length of the sample along $\hat{\mathbf{y}}$) and $\mathbf{H}_c^{\text{left, right}}$ vary linearly between the bottom and top edges.

Second, to account for flow of normal current across the boundary, the vacuum-superconductor BCs Eq. (4) are now replaced by metal-superconductor BCs Eq. (5b) [20,27] at the left and right edges, while retaining the former BCs Eq. (5a) at the top and bottom edges:

$$\nabla \times \mathbf{A} = \mathbf{H}_{\text{tot}}, \quad \left(i\nabla + \frac{1}{\kappa}\mathbf{A} \right)\psi \cdot \mathbf{n} = 0, \quad -\sigma\frac{\partial \mathbf{A}}{\partial t}\cdot \mathbf{n} = 0,$$

(5a)

$$\nabla \times \mathbf{A} = \mathbf{H}_{\text{tot}}, \quad \psi = 0, \quad -\sigma\frac{\partial \mathbf{A}}{\partial t}\cdot \mathbf{n} = \mathbf{J}_a \cdot \mathbf{n}. \quad (5b)$$

In Eq. (5b), the third BC accounts for flow of current across the boundary, and the second condition ensures that the density of superconducting electrons is zero at the edges. This ensures that the injected normal current transitions to supercurrent gradually, rather than abruptly, inside the superconductor.

C. Inclusion of Hall effect

Normal state Hall effect is a result of the conduction of electrons transverse to applied electric field. This can be incorporated in the TDGL system Eqs. (3) and (5) by rewriting the normal-state conductivity σ as a tensor:

$$\sigma = \begin{pmatrix} \sigma_{xx} & \sigma_{xy} \\ \sigma_{yx} & \sigma_{yy} \end{pmatrix} \quad (6)$$

We assume an isotropic sample ($\sigma_{xx} = \sigma_{yy}$) and by symmetry $\sigma_{yx} = -\sigma_{xy}$. To determine σ_{xx} and σ_{xy}, we use the following as the model for the normal-state conductivity [12,28]:

$$\sigma_{xx} = \sigma_0 \frac{1}{1 + \omega_c^2\tau^2}, \quad \sigma_{xy} = \sigma_0 \frac{\omega_c\tau}{1 + \omega_c^2\tau^2} \quad (7)$$

where ω_c is the cyclotron frequency $e_s(\nabla \times \mathbf{A})/m_s$ and τ is the electron scattering time. Under typical conditions, we have $\omega_c\tau \ll 1$ (low-field limit) [12,28]. Thus, $\sigma_{xx} \approx \sigma_0$ and $\sigma_{xy} \approx \omega_c\tau\sigma_0$. Due to the spatially varying magnetic field, cyclotron frequency ω_c and, consequently, σ_{xy} are also spatially varying. To enforce the low-field limit, we take $\omega_c\tau = 10^{-2}(\nabla \times \mathbf{A})$, where the prefactor of 10^{-2} ensures that $\omega_c\tau \ll 1$.

Josephson [29] proved that, macroscopically, a vortex moving at velocity $\mathbf{v}_L$ gives rise to an induced electric field $\mathbf{E} = -\frac{1}{c}\mathbf{v}_L \times \mathbf{H}$, where all the quantities are spatially and temporally averaged [9,12,13]. In the BS model [10], under an applied current $\mathbf{J}_a$, vortices experience a Lorentz force $\sim \mathbf{J}_a \times \mathbf{H}$ [9,12]. This force gives rise to velocity $\mathbf{v}_L$ along $\mathbf{J}_a \times \mathbf{H}$ and in a system such as ours (Fig. 1), this results in vortex motion along $-\hat{\mathbf{y}}$. This velocity $\mathbf{v}_L$ along $-\hat{\mathbf{y}}$ produces a field $\mathbf{E} = -\frac{1}{c}\mathbf{v}_L \times \mathbf{H}$ along $\hat{\mathbf{x}}$, the same direction as $\mathbf{J}_a$, thereby causing dissipation. However, if we were to have an additional component of $\mathbf{v}_L$ along $\hat{\mathbf{x}}$ (the same direction as $\mathbf{J}_a$), this would create a field contribution in the Hall direction. Dorsey [12] and Kopnin *et al.* [13] proved that adding a nonzero imaginary part to the relaxation parameter γ in the TDGL system Eqs. (1) produces such flux-flow contribution to the Hall field by lending the vortices a velocity component parallel to the applied current. Thus, we write $\gamma = \gamma_1 + i\gamma_2$.

In the microscopic picture, the value of γ_2/γ_1 has been shown to depend upon the electronic structure of the material [12,13]. The sign of γ_2/γ_1 determines whether vortices travel along $\mathbf{J}_a$ or against, and therefore crucially affects the sign of flux-flow contribution to Hall field. Kopnin *et al.* [13] proved that a sign reversal in Hall effect would be observed for negative values of γ_2/γ_1.

III. RESULTS AND DISCUSSION

We use COMSOL Multiphysics [30], a commercial finite element tool to numerically simulate TDGL Eqs. (3)–(5). Throughout the paper, we take GL parameter $\kappa = 2$ and normalized normal-state conductivity $\sigma_0 = 1$. In Sec. III A, we obtain a vortex state solution and propose a procedure to rigorously verify the solution to help identify any numerical errors or artifacts. In Secs. III B–III C, we study a system with externally applied current and Hall effect included. Throughout these simulations, we apply an external current $\mathbf{J}_a = 0.04\,\hat{\mathbf{x}}$. We consider six geometries: $l \times l$ square superconductors for $l/\xi \in \{3, 5, 15, 20, 100, 200\}$. We apply an external magnetic field $\mathbf{H}_{\text{ext}}$ along $\hat{\mathbf{z}}$, whose value is swept between 0 and $H_{c2} = \kappa = 2$ in steps of 0.05. For each combination of size l and $\mathbf{H}_{\text{ext}}$, we solve the modified TDGL system Eqs. (3) and (5) and compute the time-varying order parameter $\psi(\mathbf{r}, t)$ and vector potential $\mathbf{A}(\mathbf{r}, t)$. This gives us complete insight into the dynamic vortex motion and electric fields $E_x = -\partial A_x/\partial t$ and $E_y = -\partial A_y/\partial t$, which form the basis for much of our analysis.

Since we use normalized units throughout the paper, we compute the order of magnitude for these units to understand the typical physical values. We chose $\kappa = 2$, which broadly corresponds to Niobium [31]. Using the physical parameters of Nb, we compute the time units as $\sim 10^{-12}$ s [32], current density units as ~ 1 A m^{-1} [33,34], and the applied magnetic field units as ~ 1 kOe [34].

A. Vortex state and verification

We first solve TDGL Eqs. (3) on a $20\xi \times 20\xi$ planar sample (GL parameter $\kappa = 2$) with no applied current or Hall effect enabled. Thus, in this case we use the vacuum-superconductor BCs Eqs. (4) on all four sides, and observe a vortex state solution at $\mathbf{H}_{\text{ext}} = 0.9\hat{\mathbf{z}}$ (Fig. 2). We perform a thorough verification of our simulation as described in the following. First, we confirm that the simulation results are stable with respect to mesh size. We then sweep $|\mathbf{H}_{\text{ext}}|$ widely and observe the existence of both upper and lower critical fields marked by the vanishing of vortices, as expected from a type-II superconductor ($\kappa > 1/\sqrt{2}$). We also observe that for the same κ, the number of vortices increases (decreases) when the external field $|\mathbf{H}_{\text{ext}}|$ is increased (decreased). This is an expected qualitative behavior of the superconductor to let more (less) incident flux pass through the superconductor. One of the hallmarks of superconducting vortices under Ginzburg-Landau theory is *fluxoid* quantization. It states that the fluxoid value Φ' associated with each vortex is quantized by $\Phi_0 = \frac{hc}{2e}$ [18],

$$\Phi' = \Phi + \frac{4\pi}{c}\oint \lambda^2 \mathbf{J}_s \cdot dl, \quad (8)$$
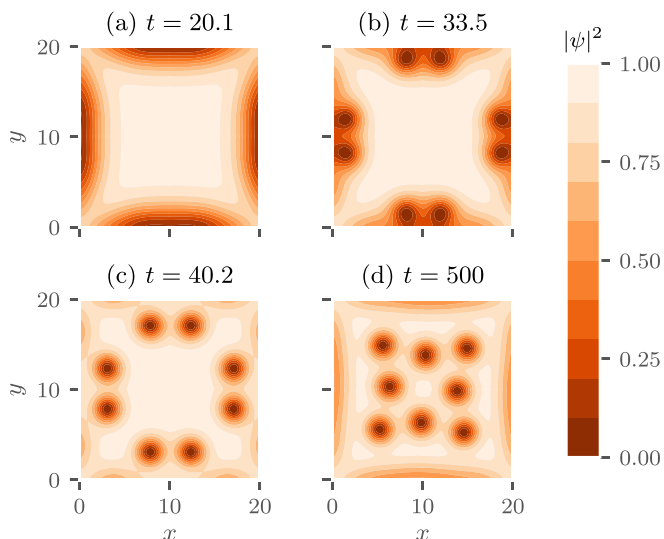
FIG. 2. $|\psi|^2$ at various instants of time, depicting major events in the formation of a vortex state in the $20\xi \times 20\xi$ sample. Applied magnetic field is $|\mathbf{H}_{\text{ext}}| = 0.9$.

where Φ is the magnetic flux $\int \mathbf{B} \cdot d\mathbf{s}$ associated with the vortex, and the integral term involving super current $\mathbf{J}_s$ and penetration depth λ is performed on a closed contour enclosing the vortex. We compute the fluxoid value and obtain $\Phi' \approx 0.96\Phi_0$ for each vortex, confirming that our simulations firmly uphold fluxoid quantization (Fig. 3).

B. Flux flow under applied current with Hall effect incorporated

In the BS model [10], magnetic vortices experience a Lorentz force under applied external current along $\mathbf{J}_a \times \mathbf{H}$ [9,12]. We apply an external current $\mathbf{J}_a = 0.04\,\hat{\mathbf{x}}$ and $\mathbf{H}_{\text{ext}}$ along $+\hat{\mathbf{z}}$, and accordingly observe vortex flow along $-\hat{\mathbf{y}}$ with vortices entering at the top edge and leaving at the bottom (Fig. 4). Consistent with the BS model, we observe faster (slower) motion of vortices with increased (decreased) magnitudes of $\mathbf{J}_a$. Choosing a larger value of $|\mathbf{J}_a|$ would increase the magnitude of current-induced magnetic field $\mathbf{H}_c$, driving the superconductor into normal state (after some time) for even
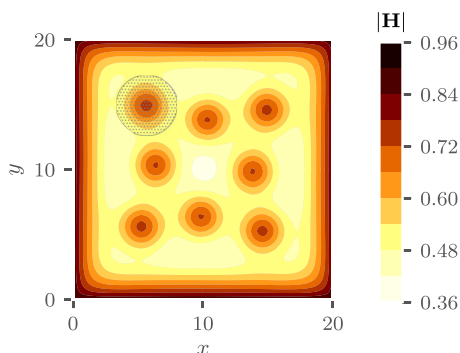

FIG. 3. We verify that the fluxoid value of each of our vortices is $\approx \Phi_0$. To compute the fluxoid value, we take a circular area centered at the vortex center defined by the local maxima in magnetic field, with a radius 2.4ξ (shown with a dotted hatch on the top-left vortex). Figure shown for $|\mathbf{H}_{\text{ext}}| = 0.9$.
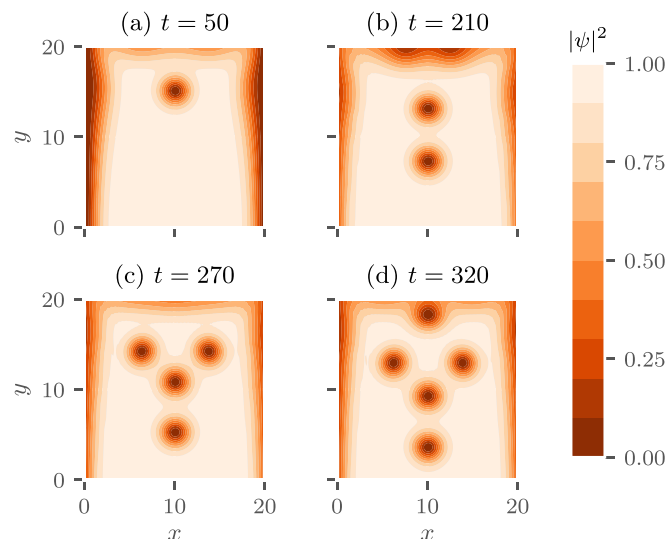

FIG. 4. We observe vortex motion under an applied external current in the transverse direction. Vortices enter at the top edge and leave at the bottom. This motion is followed by the superconductor being driven into normal state. ($|\mathbf{H}_{\text{ext}}| = 0.5$)

low values of applied field $\mathbf{H}_{\text{ext}}$. With our chosen value of $|\mathbf{J}_a| = 0.04$, we find that the system is ultimately driven into normal state for all values of $|\mathbf{H}_{\text{ext}}| \geqslant 0.35$ in the case of sizes $l/\xi \in \{15, 20\}$. For all other sizes, the system is driven into normal state for all values of $|\mathbf{H}_{\text{ext}}|$.

For sizes $l/\xi \in \{15, 20, 100, 200\}$, we observe vortices and their movement before the system eventually goes into normal state ($\psi(\mathbf{r}) = 0$), whereas for sizes $l/\xi \in \{3, 5\}$, we do not observe vortices for any value of $|\mathbf{H}_{\text{ext}}|$. To understand further, we solve the standard TDGL system Eqs. (3) and (4) (with no applied current) for $l/\xi \in \{3, 5\}$ and sweep the magnetic field $|\mathbf{H}_{\text{ext}}|$ as earlier. We do not find a vortex state solution for any value of $|\mathbf{H}_{\text{ext}}|$. We conclude that this is a size effect: the system is smaller than a critical size, forbidding the possibility of a vortex state solution.

Next, we also enable normal-state and flux-flow Hall effects following the discussion in Sec. II C, with $\gamma_2/\gamma_1 = 0.4$ and -0.4 as separate cases. The choice of $|\gamma_2/\gamma_1|$ was made in such a way that the vortices gain a perceivable amount of velocity in the direction of $\mathbf{J}_a$, but not significantly enough, so vortices still primarily move along $-\hat{\mathbf{y}}$. With Hall effect enabled, we observe complex vortex motion (Fig. 5). Vortices enter the system at the top edge and traverse smooth but irregular trajectories through the domain due to complex vortex-vortex and vortex-boundary interactions. The key difference is that they also obtain velocity in the $\pm\hat{\mathbf{x}}$ direction, unlike when Hall effect is not enabled. We seek to capture the effect of this complex motion on the longitudinal and Hall electric fields and explain the observed behavior.

C. Analysis of electric fields and Hall angle

We obtain the spatially averaged electric field by averaging across the entire domain. We find that the so-obtained $\mathbf{E}$ profiles can be grouped into three distinct types (Fig. 6). In the first type [Fig. 6(a)], the longitudinal field saturates to $\sigma_0 J_a$
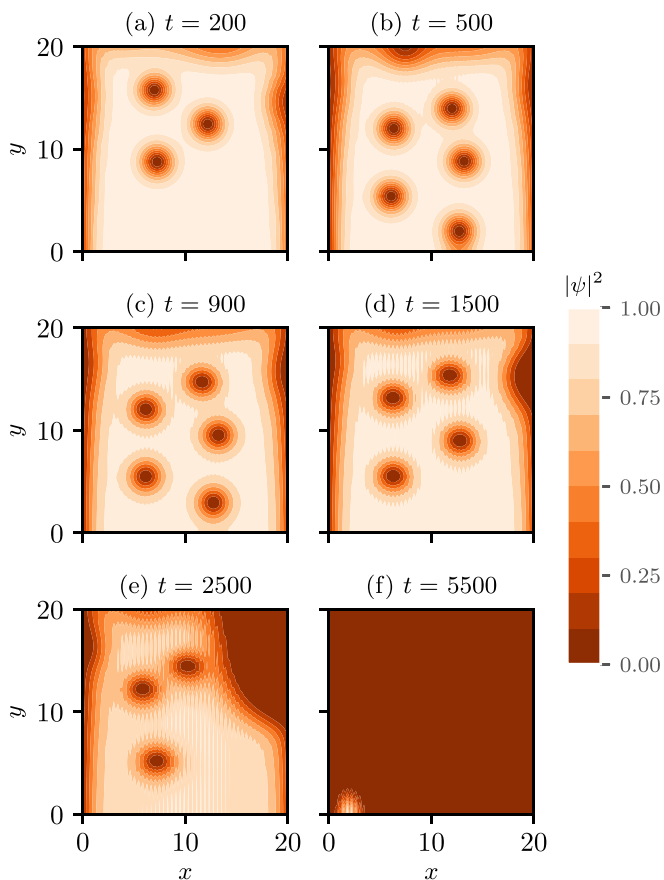
FIG. 5. Complex vortex flow under an applied external current with Hall effect enabled. The setting in normal state from the right edge starting at $t = 1500$ induces a gradual transient field largely affecting Hall behavior (Fig. 8). ($|\mathbf{H}_{ext}| = 0.5$ and $\gamma_2/\gamma_1 = 0.4$.)

(normal state) with the observation of a series of spikes prior to that. This spiking occurs due to vortex entry and exit, as discussed in Ref. [24]. The Hall field E_y also exhibits similar spiking as a result of the vortex velocity component in the direction of $\mathbf{J}_a$. Such behavior occurs for sizes $l/\xi \in \{15, 20\}$ at applied field $|\mathbf{H}_{ext}| \geqslant 0.35$ and for sizes $l/\xi \in \{100, 200\}$ at all applied fields. For fields lower than 0.35 in sizes $l/\xi \in \{15, 20\}$, the system rapidly evolves to the superconducting Meissner state with E_x reaching zero as shown in Fig. 6(b), which is the second type. Sizes $l/\xi \in \{3, 5\}$ are always driven into normal state with no vortex-related spikes. This results in the third type, with E_x saturating to $\sigma_0 J_a$ [Fig. 6(c)]. These differences in electric field behavior produce significantly different Hall effect profiles, which we address next.

We characterize the Hall effect using Hall angle, the ratio of effective transverse to longitudinal conductivity: $\tan \theta_H = \sigma'_{xy}/\sigma'_{xx}$ [12,13]. These macroscopic effective conductivities are marked with a prime to distinguish them from the normal-state quantities σ_{xx} and σ_{xy} Eqs. (7). From the macroscopic equation $\mathbf{J}_a = \sigma' \cdot \mathbf{E}$, we have

$$\begin{pmatrix} J_a \\ 0 \end{pmatrix} = \begin{pmatrix} \sigma'_{xx} & \sigma'_{xy} \\ -\sigma'_{xy} & \sigma'_{xx} \end{pmatrix} \cdot \begin{pmatrix} E_x \\ E_y \end{pmatrix}. \tag{9}$$

Thus, we get $\tan \theta_H = \sigma'_{xy}/\sigma'_{xx} = E_y/E_x$, where the fields are both spatially and temporally averaged [35]. We obtain the
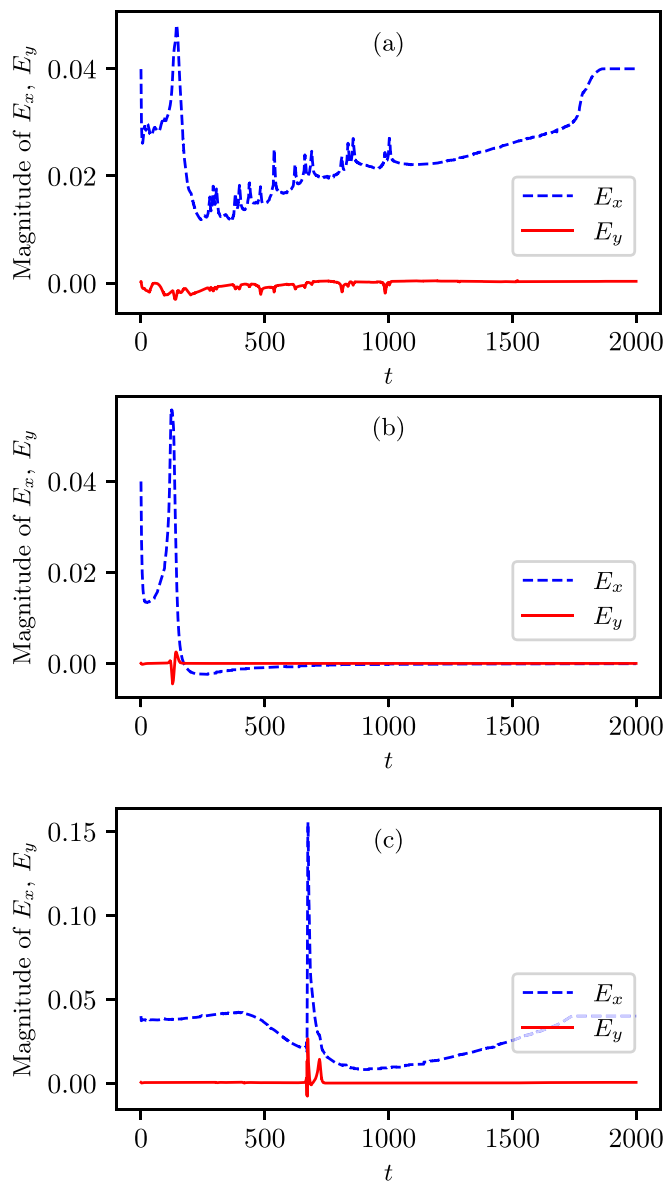

FIG. 6. The three different types of electric field profiles observed in our simulations across all sizes and magnitudes of applied field $|\mathbf{H}_{ext}|$. (a) Saturates to $\sigma_0 J_a$, exhibits spiking behavior corresponding to entry and exit of vortices from sample of size $l/\xi = 20$, and $|\mathbf{H}_{ext}| = 0.8$. (b) Saturates to 0, of sample size $l/\xi = 20$, and $|\mathbf{H}_{ext}| = 0.2$). (c) Saturates to $\sigma_0 J_a$, for sample size $l/\xi = 5$, and $|\mathbf{H}_{ext}| = 1.2$.

tangent of Hall angle $\tan \theta_H$ for each combination of applied magnetic field $|\mathbf{H}_{ext}|$ and size $l/\xi \in \{3, 5, 15, 20, 100, 200\}$ (Fig. 7). We first note that the Hall angle profiles resulting from our choice of $|\gamma_2/\gamma_1|$ closely resemble the experimental data with respect to orders of magnitude ($\tan \theta_H \sim 10^{-2}$) [8,36].

We find that as $|\mathbf{H}_{ext}| \rightarrow H_{c2}$, when the superconductor is rapidly driven into normal state, Hall angle varies linearly with $|\mathbf{H}_{ext}|$, as in the case of normal metals. In this regime, flux-flow contribution is negligible and all sizes $l/\xi \in \{3, 5, 15, 20, 100, 200\}$ have the same profile. This is in agreement with expected behavior because we do not have any size effect for normal metals. When $|\mathbf{H}_{ext}| \approx 0$, the Hall angle
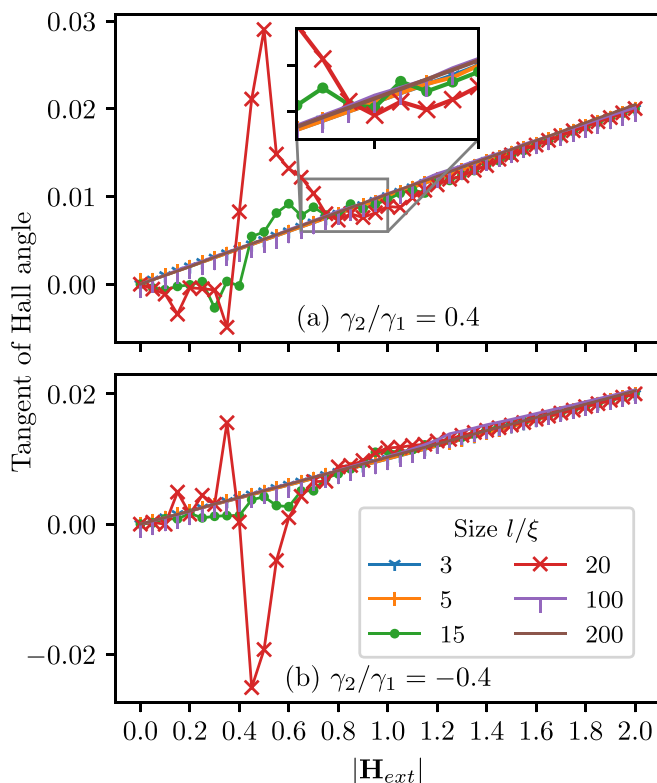
FIG. 7. (a) Hall angle profiles for $\gamma_2/\gamma_1 = +0.4$. (b) Hall angle profiles for $\gamma_2/\gamma_1 = -0.4$. Evidently, size is an important parameter in determining Hall behavior, with the smallest size $l/\xi = 3$ behaving identical to a normal conductor. Sign reversal is only seen for $l/\xi = 20$, in which case $\gamma_2/\gamma_1 = 0.4$ and -0.4 show opposite behavior. Fields are averaged till $t = 11000$, starting after the initial transient has subsided (Fig. 6).

approaches 0. At these low fields, sizes $l/\xi \in \{3, 5\}$ are driven to normal state. As normal metals, they have negligible Hall fields at $|\mathbf{H}_{\text{ext}}| \approx 0$ and, consequently, a very small Hall angle. On the other hand, sizes $l/\xi \in \{15, 20\}$ are in the superconducting state at these low fields and therefore have negligible E_y and E_x. The bulk sizes $l/\xi \in \{100, 200\}$ are in the vortex state and both the normal Hall field, and flux-flow contribution are small at low fields. Thus, although the Hall angle is small for all groups of sizes at $|\mathbf{H}_{\text{ext}}| \approx 0$, the underlying states are different.

We see that the Hall angle profile is completely linear for sizes $l/\xi \in \{3, 5\}$. This is a result of them behaving as normal metals with no vortex state, and electric field $E_x(t)$ saturating to $\sigma_0 J_a$ for all values of $|\mathbf{H}_{\text{ext}}|$ [third type shown in Fig. 6(c)].

We next look at sign reversal of Hall angle, a key anomaly in the Hall behavior of some superconductors. For sizes $l/\xi \in \{15, 20\}$, we observe a region of sharp deviation from linear, normal-conductor behavior for intermediate values of applied field, i.e., around $|\mathbf{H}_{\text{ext}}| \approx 0.5$ (Fig. 7). This is the region where flux-flow contribution to the Hall effect is most significant because for higher fields, normal state sets in rapidly, and for lower fields, there are no vortices (Meissner state). We find that strong, negative flux-flow contribution leads to sign reversal for $\gamma_2/\gamma_1 = -0.4$, and positive contribution leads to a peak for $\gamma_2/\gamma_1 = 0.4$, in agreement with Kopnin *et al.* [13].
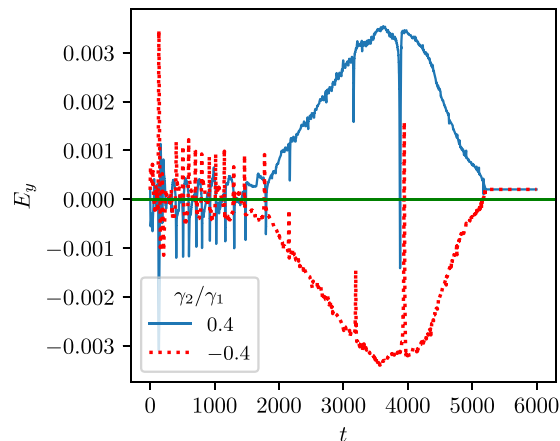

FIG. 8. E_y fields for size $l/\xi = 20$ at $|\mathbf{H}_{\text{ext}}| = 0.5$ The gradual transients starting at $t \approx 1500$ are responsible for the vastly different Hall angle for $\gamma_2/\gamma_1 = 0.4$ and -0.4. Similar transients are seen for $|\mathbf{H}_{\text{ext}}| \approx 0.5$, leading to the Hall angle profile in Fig. 7.

To understand the precise transient behavior leading to this vast difference, we look at the spatially averaged fields E_x and E_y as functions of time (for $|\mathbf{H}_{\text{ext}}| = 0.5$). First, we find that for both $\gamma_2/\gamma_1 = 0.4$ and -0.4, E_x has an identical profile. This is expected because γ_2 only influences the motion of vortices along $\mathbf{J}_a$, thus affecting only E_y (Sec. II C). On the other hand, we find significant differences in $E_y(t)$ profiles (Fig. 8). It is evident that the difference in Hall behavior between $\gamma_2/\gamma_1 = 0.4$ and -0.4 can be attributed almost entirely to the transients starting at $t \approx 1500$. Although spiking behavior results in peaks in the opposite direction, they have negligible contribution to the average. Instead, the gradual transient starting at $t \approx 1500$ leads to different profiles for $\gamma_2/\gamma_1 = 0.4$ and -0.4, giving a strong positive and negative contribution to Hall field, respectively. We try to relate this transient with order parameter (Fig. 5) to determine the precise behavior causing such transients. We find that this transient is the induced field resulting from variation in $\mathbf{A}$ during the onset of normal state (Fig. 5). This onset occurs from the right boundary for $\gamma_2/\gamma_1 = 0.4$ (as seen in Fig. 5), and from the left for $\gamma_2/\gamma_1 = -0.4$ (Fig. 8). For both $\gamma_2/\gamma_1 = 0.4$ and -0.4, this transient leads ultimately to saturation of E_y to the same, small positive value. This is the non-flux-flow, or normal-state contribution to the Hall field. Interestingly, we find that although size $l/\xi = 15$ exhibits vortex behavior similar to $l/\xi = 20$, we do not find sign reversal in Hall angle. This is due to the suppressed gradual transient fields in $l/\xi = 15$, leading to a much weaker contribution of flux-flow Hall effect.

Lastly, we look at the bulk sizes $l/\xi \in \{100, 200\}$, which show a completely linear Hall profile. Although these sizes are in the vortex state at every value of applied field, we see negligible flux-flow contribution to Hall effect. We find that these sizes have highly suppressed peaks in the electric field induced by vortex motion. This can be attributed to the decreased effect of vortex entry/exit on the spatially averaged electric fields due to the large superconductor area. Further, the onset of normal state as described in the previous paragraph occurs nearly equally from both the left and right

boundaries, which can perhaps be attributed to the decreasing role of the boundary as we move toward the bulk regime. These two factors ensure that flux-flow contribution is negligible, resulting in a linear Hall angle profile. Therefore, it is evident that along with γ_2 (whose value depends on the electronic structure) and several other parameters, size influences Hall behavior significantly, adding to the reasoning behind the observation of a diverse variety of Hall angle profiles in various materials.

Anomalous Hall effect in superconductors has been an open theoretical problem and there exist alternate theories that seek to explain this phenomenon, besides the one used in this study. Recently, Auerbach and Arovas [37] proposed a model based on moving vortex charge (MVC) and refuted the imaginary relaxation constant model. It was previously shown that vortices could carry charge [38], and therefore their motion in the Hall direction alone would create a contribution to the Hall current. Thus, in a vortex imaging setup if we find that Hall angle is reversed while vortices move strictly perpendicular to the current, it would validate the MVC theory. However, if vortices move in both directions, the result would be inconclusive.

In summary, we have simulated the anomalous Hall effect using the modified TDGL equations in COMSOL Multiphysics and shown that the solutions provide insights into the precise temporal dynamics of transient fields and vortex behavior that scale with the sample size. We have explored theoretically how features of the anomalous Hall effect evolve with a variation of the linear dimensions when the lengths are only a few times the coherence length. The Hall effect behavior predicted by these simulations may be probed with advanced experimental techniques that have already been applied to image vortices [1–6,39]. Transport experiments on superconducting nanowires with widths ranging from a few hundred [40,41] to tens of nanometres (a few times the coherence length) [42] have been reported. It is now practically feasible to fabricate systems of small widths as discussed in our paper. Such studies would be important for understanding finite-size effects in superconductors and their evolution at microscopic length scales.

[1] Y. Schlussel, T. Lenz, D. Rohner, Y. Bar-Haim, L. Bougas, D. Groswasser, M. Kieschnick, E. Rozenberg, L. Thiel, A. Waxman, J. Meijer, P. Maletinsky, D. Budker, and R. Folman, Wide-field imaging of superconductor vortices with electron spins in diamond, Phys. Rev. Appl. **10**, 034032 (2018).

[2] L. Thiel, D. Rohner, M. Ganzhorn, P. Appel, E. Neu, B. Müller, R. Kleiner, D. Koelle, and P. Maletinsky, Quantitative nanoscale vortex imaging using a cryogenic quantum magnetometer, Nat. Nanotechnol. **11**, 677 (2016).

[3] A. Kremen, S. Wissberg, N. Haham, E. Persky, Y. Frenkel, and B. Kalisky, Mechanical control of individual superconducting vortices, Nano Lett. **16**, 1626 (2016).

[4] L. Embon, Y. Anahory, Z. L. Jelić, E. O. Lachman, Y. Myasoedov, M. E. Huber, G. P. Mikitik, A. V. Silhanek, M. V. Milošević, A. Gurevich, and E. Zeldov, Imaging of super-fast dynamics and flow instabilities of superconducting vortices, Nat. Commun. **8**, 85 (2017).

[5] B. Raes, J. Van de Vondel, A. V. Silhanek, C. C. de Souza Silva, J. Gutierrez, R. B. G. Kramer, and V. V. Moshchalkov, Local mapping of dissipative vortex motion, Phys. Rev. B **86**, 064522 (2012).

[6] D. Cole, S. Bending, S. Savel'ev, A. Grigorenko, T. Tamegai, and F. Nori, Ratchet without spatial asymmetry for controlling the motion of magnetic flux quanta using time-asymmetric drives, Nat. Mater. **5**, 305 (2006).

[7] S. N. Artemenko, I. G. Gorlova, and Y. I. Latyshev, Vortex motion and Kosterlitz-Thouless transition in superconducting single crystals $Bi_2Sr_2CaCu_2O_x$, Phys. Lett. A **138**, 428 (1989).

[8] Y. Iye, S. Nakamura, and T. Tamegai, Hall effect in high temperature superconductors near T_c, Physica C: Superconductivity **159**, 616 (1989).

[9] S. J. Hagen, C. J. Lobb, R. L. Greene, M. G. Forrester, and J. H. Kang, Anomalous Hall effect in superconductors near their critical temperatures, Phys. Rev. B **41**, 11630 (1990).

[10] J. Bardeen and M. J. Stephen, Theory of the motion of vortices in superconductors, Phys. Rev. **140**, A1197 (1965).

[11] P. Nozières and W. F. Vinen, The motion of flux lines in type II superconductors, Philos. Mag. **14**, 667 (1966).

[12] A. T. Dorsey, Vortex motion and the Hall effect in type-II superconductors: A time-dependent Ginzburg-Landau theory approach, Phys. Rev. B **46**, 8376 (1992).

[13] N. B. Kopnin, B. I. Ivlev, and V. A. Kalatsky, The flux-flow Hall effect in type II superconductors. an explanation of the sign reversal, J. Low Temp. Phys. **90**, 1 (1993).

[14] Q. Du and P. Gray, High-Kappa Limits of the time-dependent Ginzburg-Landau model, SIAM J. Appl. Math. **56**, 1060 (1996).

[15] Q. Du, Numerical approximations of the Ginzburg-Landau models for superconductivity, J. Math. Phys. **46**, 095109 (2005).

[16] L. P. Gor'kov and N. B. Kopnin, Vortex motion and resistivity of type-II superconductors in a magnetic field, Sov. Phys. Usp. **18**, 496 (1975).

[17] L. D. Landau and V. L. Ginzburg, On the theory of superconductivity, Zh. Eksp. Teor. Fiz. **20**, 1064 (1950) [73 - On the theory of superconductivity, in *Collected Papers of L.D. Landau*, edited by D. T. Haar (Pergamon, 1965), pp. 546–568].

[18] M. Tinkham, *Introduction to Superconductivity*, 2nd ed. (McGraw-Hill Inc., New York, 1996).

[19] J. Deang, A study of inhomogeneities and anisotropies in superconductors via ginzburg-landau type models, Ph.D. thesis, Virginia Polytechnic Institute and State University, Blacksburg, VA, 1997.

[20] M. Ögren, M. P. Sørensen, and N. F. Pedersen, Self-consistent Ginzburg-Landau theory for transport currents in superconductors, Physica C: Superconductivity **479**, 157 (2012), Proceedings of VORTEX VII Conference.

[21] T. S. Alstrøm, M. P. Sørensen, N. F. Pedersen, and S. Madsen, Magnetic flux lines in complex geometry Type-II superconductors studied by the time dependent Ginzburg-Landau equation, Acta Appl. Math. **115**, 63 (2011).

[22] S. Chapman, Q. Du, M. Gunzburger, and J. Peterson, Simplified Ginzburg-Landau models for superconductivity valid for high kappa and high fields, Adv. Math. Sci. Appl. **5**, 193 (1995).

[23] Solution to the full problem provides insight into physical processes in the exterior of the sample, e.g. possibility of evanescent waves, which we expect to not affect the interior flux-flow physics that are the focus of our work.

[24] M. Machida and H. Kaburaki, Direct Simulation of the Time-Dependent Ginzburg-Landau Equation for Type-II Superconducting Thin Film: Vortex Dynamics and V-I Characteristics, Phys. Rev. Lett. **71**, 3206 (1993).

[25] W. D. Gropp, H. G. Kaper, G. K. Leaf, D. M. Levine, M. Palumbo, and V. M. Vinokur, Numerical simulation of vortex dynamics in type-II superconductors, J. Comput. Phys. **123**, 254 (1996).

[26] T. Winiecki and C. S. Adams, Time-dependent Ginzburg-Landau simulations of the voltage-current characteristic of type-II superconductors with pinning, Phys. Rev. B **65**, 104517 (2002).

[27] D. Vodolazov, B. J. Baelus, and F. M. Peeters, Dynamics of the superconducting condensate in the presence of a magnetic field. Channelling of vortices in superconducting strips at high currents, Physica C: Superconductivity **404**, 400 (2004), Proceedings of the Third European Conference on Vortex Matter in Superconductors at Extreme Scales and Conditions.

[28] C. Hurd, *The Hall Effect in Metals and Alloys* (Plenum Press, New York, 1972).

[29] B. D. Josephson, Potential differences in the mixed state of type II superconductors, Phys. Lett. **16**, 242 (1965).

[30] *COMSOL Multiphysics Reference Manual, v5.4*, COMSOL AB, Stockholm, Sweden (2018), https://doc.comsol.com/5.4/doc/com.comsol.help.comsol/COMSOL_ProgrammingReferenceManual.pdf.

[31] D. K. Finnemore, T. F. Stromberg, and C. A. Swenson, Superconducting properties of high-purity niobium, Phys. Rev. **149**, 231 (1966).

[32] B. Oripov and S. M. Anlage, Time-dependent Ginzburg-Landau treatment of rf magnetic vortices in superconductors: Vortex semiloops in a spatially nonuniform magnetic field, Phys. Rev. E **101**, 033306 (2020).

[33] Y. Asada and H. Nosé, Superconductivity of niobium films, J. Phys. Soc. Jpn. **26**, 347 (1969).

[34] S. J. Williamson and L. E. Valby, Nonlocal Characteristics of the Bulk Upper Critical Field of Niobium, Phys. Rev. Lett. **24**, 1061 (1970).

[35] We perform time averaging after the initial transient spike has subsided (Fig. 6) because the TDGL dynamics right after initialization is unphysical. As an aside, we also note that there is an inappreciable difference in the results on the Hall angle profiles between the delayed averaging and averaging from $t = 0$.

[36] L. Forró and A. Hamzić, Flux-flow Hall effect in $YBa_2Cu_9O_7$ and $Bi_2Sr_2CaCu_2O_8$ high temperature superconductors, Solid State Commun. **71**, 1099 (1989).

[37] A. Auerbach and D. P. Arovas, Hall anomaly and moving vortex charge in layered superconductors, SciPost Phys. **8**, 061 (2020).

[38] D. I. Khomskii and A. Freimuth, Charged Vortices in High Temperature Superconductors, Phys. Rev. Lett. **75**, 1384 (1995).

[39] S. E. Lillie, D. A. Broadway, N. Dontschuk, S. C. Scholten, B. C. Johnson, S. Wolf, S. Rachel, L. C. L. Hollenberg, and J.-P. Tetienne, Laser modulation of superconductivity in a cryogenic wide-field nitrogen-vacancy microscope, Nano Lett. **20**, 1855 (2020).

[40] I. V. Grigorieva, A. K. Geim, S. V. Dubonos, K. S. Novoselov, D. Y. Vodolazov, F. M. Peeters, P. H. Kes, and M. Hesselberth, Long-Range Nonlocal Flow of Vortices in Narrow Superconducting Channels, Phys. Rev. Lett. **92**, 237001 (2004).

[41] F. Otto, A. Bilušić, D. Babić, D. Y. Vodolazov, C. Sürgers, and C. Strunk, Reversal of Nonlocal Vortex Motion in the Regime of Strong Nonequilibrium, Phys. Rev. Lett. **104**, 027005 (2010).

[42] R. Córdoba, P. Orús, Z. L. Jelić, J. Sesé, M. R. Ibarra, I. Guillamón, S. Vieira, J. J. Palacios, H. Suderow, M. V. Milosević, and J. M. De Teresa, Long-range vortex transfer in superconducting nanowires, Sci. Rep. **9**, 12386 (2019).